Photometric monitoring of cataclysmic variables

Abstract

The first objective of this project was to properly obtain data on the brightness changes of interacting stars known as cataclysmic variables, by means of usual amateur astronomical equipment. Those brightness changes had to be monitored on several time scales in order to detect eventual subtle variations, both in the short- and the long-term. Considering that the author had no photometry experience at all (barely some short CCD-imaging practice), this endeavour resulted a very hard – but totally enlightening, enjoyable, and fascinating – challenge.

The second objective was to analyze the obtained images, trying to infer correct and valuable scientific information from it. This desk part also required a lot of work, since after suitable processing of images there still remained a large and careful detective-style analysis. Fortunately, very interesting information about the monitored cataclysmic stars could be found – both qualitative and quantitative. Finally, the comparison to published data corroborated the real potential of serious amateur work, even though performed by means of modest equipment.

1 – Introduction

Cataclysmic variable (CV) stars are pairs of stars that orbit so closely[1] that stellar material actually flows between them, usually from a red giant main sequence star to a compact white dwarf. Such accretion can cause the white dwarf to go into outburst, and that is the origin of this stellar type denomination. The most massive star of the binary system is called the primary, and the other the secondary.

The lightcurve of CVs is dominated by the flow of stellar material from one star to the other, which can outshine the two stars themselves. In order that material from one star can flow towards the other, the net gravitational force at the surface of the donor star has to be oriented towards the other star – a situation technically defined as the size of the donor star being larger than its *Roche lobe* – and the system is called a *semidetached binary.*

CVs can be roughly divided into *novae* and *dwarf novae*. Novae are white dwarfs that experience a sudden outburst in a surface layer as a consequence of the excessive accreted material, while the outburst of dwarf novae is due to a brightening of the accretion disk itself. It is expected that dwarf novae would eventually become novae, but no dwarf novae has done so since they were discovered **[1]**.

Novae can be further divided into *classical novae* (just only one known explosion) or *recurrent novae* (multiple observed outbursts). The dwarf novae family is much more prolific, being the most important ones: *nova-likes* (the disk permanently in outburst), *polars* (the white dwarf has a magnetic field strong enough to prevent the formation of an accretion disk[2]), *AM Her* (an almost no interfering magnetic field), and *intermediate polars* (a magnetic field that variably interacts with the accretion disk).

CVs can be relied upon to vary continuously and unpredictably, never exactly repeating themselves. They may fade by a factor of ten from one cycle to the other, only to recover another cycle later. They do exhibit a rhythmic pulse, brightening and fading in correspondence with their particular orbital period, but they also show a permanent and irregular flickering **[2]**.

Considering that CV monitoring provides valuable information on the final stages of stellar evolution, accretion phenomena, and accretion disk properties **[3]** on an interesting time scale and over a wide statistical sample, not in vain it appears as one of the frequent tasks of the professional's latest satellites and observatories. Also for amateurs such monitoring becomes a rewarding activity, regarding CVs noticeable variability.

For creating a likely model of a given CV system, observational data becomes essential. At the time of this writing there are 650 CVs known, plus some other 250 related objects[3] **[4]**, simply too many for the professionals to monitor them continuously. This is where the record of serious amateur observations can become truly worthy, on condition that such data has been properly obtained and processed.

---

[1] Typically the orbital distance is lesser than one solar diameter.

[2] The accretion takes place through a magnetically controlled column that funnels mass onto one (or both) of the white dwarf's magnetic poles.

[3] They are semidetached binaries having either a neutron star or black hole primary instead of a white dwarf, or detached binaries consisting of either a white dwarf or a white dwarf precursor primary **[4]**.

2 – Equipment

All the photometric monitoring tasks of CV targets for this project were performed by the author from mid April to early June, 2007, working alone at his recently finished observatory. The observatory is called OLASU [4], and is placed in the suburbs of Salto, Uruguay (31° 23' South, 57° 59' West), where about 250,000 inhabitants live in the area. Prior to this project the author had no experience at all about doing photometry.

The main telescope of OLASU, shown in Fig.1, is an improved version of a classical Schmidt-Cassegrain [5] (Meade LX-200R), having 30 cm of diameter and f/10 of focal ratio. It is permanently mounted on a fixed pier housed under a steel dome of 3.6 m, having an acceptable equatorial alignment. The dome has no robotic control.

Despite the telescope been trained to minimize its tracking errors before the beginning of the monitoring tasks, it still presented a great error (about 50 arcsec from peak to peak) along all this project. This handicap severely limited the exposure time of images due to noticeable star trailing. Unfortunately, there was not physical possibility to perform autoguiding (a technique that would have dramatically reduced such trouble).

The CCD camera, shown in Fig. 2, is a modest amateur monochrome camera (Meade DSI PRO II) without any particular chip refrigeration other than a large metallic-plate dissipater, and no binning capacity. The active area of the CCD is 752-pixel columns x 582-pixel rows, each pixel measuring 8.6 (horizontal) x 8.3 (vertical) m m.

The remaining imaging equipment worth mentioning for this project includes two focal reducers (f/6.3 and f/3.3) of satisfactory quality. Towards the very end of the imaging period, Bessel photometric filters (Schuler filters Blue, Visible, Red and Clear, supplied by Astrodon) were definitively incorporated to the observatory, although still lacking an automatic filter wheel (filters had to be placed on a manual sliding tray, as Fig. 2 shows).

The imaging software (called Meade Autostar Suite) is supplied altogether with the CCD camera by its manufacturer. The used version for this project was 3.23, running in a nearby laptop computer, operating under Windows 2000 Professional Operating System.

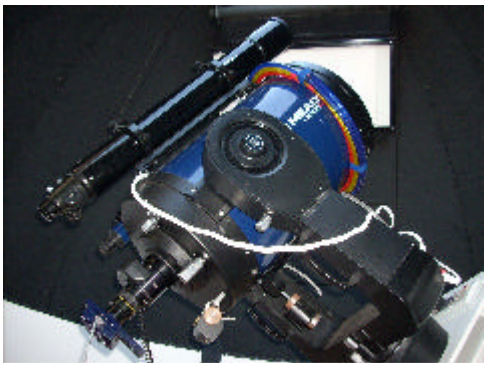

Fig 1: The telescope and the flat dome.

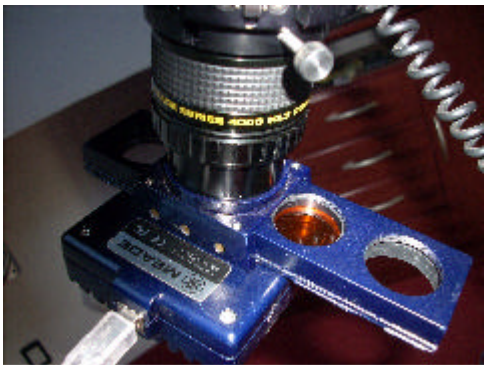

Fig 2: The CCD and f/3.3 focal reducer.

[4] OLASU stands for "*Observatorio Los Algarrobos, Salto, Uruguay*".
[5] Although the manufacturer pompously (and rather tricky) called it "*Advanced Ritchey-Chretien*".

Given the particular available equipment, the *field of view* (also called the *image scale*) of the corresponding CCD images, expressed in arcsec, becomes **[5]**:

$$FOV = \frac{CCD \cdot size \cdot x \cdot 206,265}{effective \cdot focal \cdot length}$$

Then, using no focal reducer (that is, working at f/10) the corresponding image scale results 7.3 x 5.4 arcmin, and the sky area covered by each single pixel is (for the long side) 0.58 arcsec/pix. The same values working with the f/6.3 focal reducer gives an image scale of 11.6 x 8.7 arcmin and a pixel scale of 0.92 arcsec/pix, and for the f/3.3 focal reducer 22.1 x 16.5 arcmin and 1.8 arcsec/pix respectively.

Ideally, each pixel should cover no more than half the size of the FWHM of the stellar profile [6] (a smaller pixel scale – *oversampling* – increases noise, while a larger pixel scale – *undersampling* – decreases photometry accuracy **[6]**). Regarding that the average seeing – the degree of atmospheric turbulence – at OLASU is typically between 3 to 4 arcsec[7], hence the most sensible pixel scale to work with becomes 1.75 arcsec/pix.

Based on such objective consideration, along this project all the images were taken with the help of the f/3.3 focal reducer. Fortunately, not only it collaborated by optimizing photometry accuracy (at least, theoretically [8]), but at the same time it allowed to image at "larger" exposure times by minimizing star trailing (the smaller the focal length, the larger the covered sky area, hence the lesser the incidence of tracking errors).

As an aside and final bonus, working at f/3.3 also greatly facilitated the tedious and difficult practical task of properly placing CV targets right on the tiny CCD field. (Despite the telescope becoming "faster" and contrary to popular belief, for stellar targets like the ones of this project the required exposure time for obtaining a given brightness level of their "point-like" formed images remains exactly the same, as it depends only on the telescope's aperture and not on its focal ratio **[7]**.)

Due to poor tracking accuracy already mentioned, the maximum acceptable exposure time (defined as obtaining at least 40% of suitable images even for the forgiving photometry technique), working with the f/3.3 focal reducer resulted about 90 seconds.

Other than some light absorption and distortion, the drawback of working with the f/3.3 focal reducer is that star fields becomes more concentrated – stars appear much more closer ones from another – so that photometry become inherently more inaccurate.

At Appendix I it is presented the transmission curves of the telescope, CCD camera and photometric filters.

[6] A photometric stellar profile is commonly described by its width when the intensity has dropped to half the peak value, that is, its *full width at half maximum*, or simply FWHM). The FWHM greatly depends on the atmospheric seeing, precision of the focus, quality of the optics, and telescope tracking during the exposure.
[7] As that is the average range of FWHM of a star profile of good SNR obtained from here on a CCD image.
[8] In practice focal reducers do introduce a piece of glass that absorbs and scatters some light, so somehow always distorting the field.

3 – Experimental technique

Before attempting any photometry measurement, any CCD image has to be "normalized" or "calibrated". This task aims to the elimination (or at least, to maximal reduction) of all distortions – technically referred to as *noise* – that both the CCD camera and optical system have inevitably introduced in the captured images.

In the case of amateur equipment, as the one used in this project, the main causes of noise come from (a) a uniform response ("hot pixels") that the CCD camera autogenerates independently of the incoming light but depending on the CCD temperature and the exposure time, and (b) non-uniform responses from pixels and electronics of the CCD camera and also from optical irregularities or randomly distributed dirties of the overall system. Fortunately, both types of distortion can be easily and correctly removed.

For a given image, hot pixels are eliminated by subtracting a *master dark frame* (a combined frame of several images taken at the same CCD temperature and the same exposure time of the considered image, but with no light entering the camera), while all non-uniform responses are eliminated by dividing by a *master flat field* (a combined frame of several images of a perfectly even illuminated field, each one free of hot pixels).

Therefore, applying just the right dark frames and flat fields the original CCD image becomes calibrated and ready for photometry. Photometry is the process of measuring the brightness of a luminous source. As measuring implies the comparison to an arbitrary given standard, basically there are two methods to perform photometry on stars – that is, to find out their particular magnitudes.

On the one hand, the technique used more often by the professionals, namely *all-sky photometry*, is based on comparing with extreme care the star in question to several widely spaced stars whose brightness is precisely known, which allows finding out a final value. On the other hand, the easiest to perform, namely *differential photometry*, is based on measuring the brightness difference between a target star to several nearby stars, thus finding out not a final value but just a difference.

Despite its simplicity, differential photometry provides the most accuracy when measuring small variations, such as is the usual case of CV stars – the amplitude of their ligthcurves is typically well under 0.3 magnitudes. This is the method that has been applied extensively along this work, with comparison stars always in the same image as the target.

Comparison stars always in the same field means that all of the stars and target have very similar air masses[9], so that atmospheric extinction effects cancel out providing that the stars and the target are similar in colour **[8]**. If comparison stars are distinctly different in colour, extinction effects may not be able to properly compensate each other, especially if working with fields below 30° altitude.

[9] The air mass is a measure of the particular length of the Earth's atmosphere that the light path from a given star has to travel in order to reach us. Such path not only attenuates the incoming light, but also affects it variably according to its wavelength (the atmosphere scatters and attenuates blue light more than red).

There are several programs that perform differential photometry. They all are based on measuring the relative light signal strength (*pixel values*) received on a linear device (CCD) during the exposure time. This is automatically accomplished by means of a software tool called *aperture photometry.*

All that aperture photometry requires is the setting of three concentric radial[10] parameters: the radius of an inner circle adjusted around the star, where the star's pixels are to be measured (sometimes called the *aperture*); and the radius of a second and a third circle which defines a dead zone where there is no light from the star, just background light (usually called the *annulus*).

All that aperture photometry does is to count both the pixel values inside the aperture and inside the annulus, and subtract the latter from the former. This simple procedure gives the photometric value for each considered star, usually referred to as the *raw instrumental magnitudes*, as they still depends on the particular imaging system and the conditions at the imaging time **[9]**.

The basic idea supporting differential photometry is that all imaging peculiarities will counterbalance when considering just the difference among raw instrumental magnitudes of two field stars of the same magnitude and colour, obtained by means of the same measurement process. The objective of obtaining a precise lightcurve of a given CV adds the issue that the comparison star has obviously to be non-variable.

In order to minimize this problem, the natural solution is to work not with one, but with several comparison stars – usually refer to as *check stars* – some slightly brighter and some slightly fainter that the expected peak swings of the variable in question. This allows eliminating any comparison stars that happen to minimally vary, and improving the accuracy of the photometry difference values along the imaging session.

[10] Aperture photometry is usually performed by means of circles, but the technique works the same for ellipses or rectangles. As a matter of fact, several photometry software allow the user to select such form.

4 – Selection of the most suitable CV targets

The selection of the right cataclysmic variables to be photometric monitored along this project was a matter of the utmost importance. Given the particular time period and site location from where the monitoring was to be done, and the modest capabilities of the equipment to be used, the full spectrum of potential cataclysmic targets became severely reduced. Specifically, CV candidates had to simultaneously fulfill the following requisites.

In the obvious first place, the stars had to properly appear in the night sky. As this observational project was to be done from early April to early June (southern hemisphere's autumn), the first restriction imposed to CV candidates was that their right ascension (RA) had to be between 9 and 15 hours (that is, assuring convenient transit times: between 21:00 to 03:00 hours for early April, to between 17:00 to 23:00 hours for early June).

A second restriction came from the fact that photometric measurements had to be essentially free of variable atmospheric extinction. This meant imaging CVs only when placed at altitudes higher than 45° (airmasses lesser than 1.414). Considering that the latitude of the observational site was 31° S, and that the targets had to be at the requested altitude in the sky for a minimum of 4 straight hours (the largest, the better), this implied that the candidate's declination (DEC) had to be at least lesser than 0 degree (the furthest negative, the better).

The third need was that orbital periods of the CVs had to be as short as possible, so that at least one full cycle of corresponding lightcurves could be obtained during a single imaging session.

The last restriction was forced by equipment limitations. Regarding the lack of a good tracking system or autoguiding possibilities, exposure times had to be as shorter as possible. The natural solution was to select CVs as brighter as possible.

Having defined the target requirements, the next step was to find out which CVs potentially applied. Such investigation was made using the *Catalogue of Cataclysmic Binaries, Low-Mass X-Ray Binaries and Related Objects* by Hans Ritter and Ulrich Kolb is a complete and up-to-date cataclysmic variable stars compendium. Its last edition (7.7) includes literature published up to 30 September 2006, containing entries for 647 known cataclysmic binaries, 85 known low-mass X-rays binaries, and 169 "related objects" (detached binaries where the primary is a white dwarf, thus making the system a potentially "pre-cataclysmic" binary).

After a thoughtful analysis, the following five CVs were finally selected as the most suitable targets for this project, in merit to also represent different cataclysmic types:

CV star	*Type of CV*	*RA (J2000)*	*DEC (J2000)*	m_V *(min)*	*Orb. period*
T Pyx	recurrent nova	09h 04m 41.5s	-32° 22' 47.1"	14.9	1h 45m
HW Vir	detached system	12h 44m 20.3s	-08° 40' 16.1"	11.5	2h 48m
EX Hya	intermediate polar	12h 52m 24.4s	-29° 14' 57.1"	14.0	1h 38m
AB Nor	dwarf nova	15h 49m 15.5s	-43° 04' 49.1"	17.5	2h 00m

V1223 Sgr	intermediate polar	18h 55m 02.2s	-31° 09’ 49.1”	16.8	3h 22m

5 – Data reduction

The monitoring of the CV targets was performed along ten imaging sessions, from April 19th to June 4th, 2007. All taken images appear summarized at the table presented in Appendix 2. In particular, EX Hya and HW Vir were monitored on several times (along respectively 6 and 4 sessions) in order to eventually detect some variability at longer (weeks-scale) spans than the ready noticeable at any session (minutes-scale).

The process of finding each CV target was performed with the indispensable aid of stellar images obtained from *The STScI Digitized Sky Survey* at http://stdatu.stsci.edu/cgi-bin/dss_form. From its website it was possible to download images exactly centered on each desired CV, at a very suitable scale of 15 x 15 arcmin (almost like the CCD field).

The exposure time of each image was selected as the minimum that allowed obtaining a proper dynamic range (brightest stars in the field with pixel counts about 70% of the maximum possible, in order to not distort measurements), as long as it did not overpass the 90-second poor-tracking limit. Unfiltered images met such condition in less than one minute, while filtered images had to be taken at the maximum exposure time.

All images were obtained from targets at a minimum altitude of 45°. All the images were stored in uncompressed format (FITS), with also supports the corresponding imaging information. The complete log of all imaging sessions is presented at Appendix II.

At the same time each image was taken and stored, the imaging software already applied the corresponding dark frames from a master-dark bank previously and properly obtained. Flats were taken on each session at a dome frame. Later, flat corrections were performed at the time of photometry measurement, done with the software *Canopus*.

Five comparison stars – the maximum that *Canopus* allows – were always used for performing the corresponding differential photometry. The very first thing to do at the analysis stage was to discard all images that stars appeared notoriously trailed (Canopus presents each image in order to be either accepted or rejected). After finishing photometry, *Canopus* presented the ligthcurve of each comparison star.

The second image rejection came from eliminating those images where the corresponding points in comparison ligthcurves were notoriously separated from the main curves. This examination also permitted to check the proper stability of the selected comparison stars. After this process, the raw instrumental magnitudes of the CV target and the five comparison stars were put on an excel spreadsheet (one spreadsheet for every CV, thus containing data from all different sessions for the same target).

Canopus allows to export the following data: Julian date (either heliocentric corrected or not[11]), civil date, UT time, air mass, seven raw instrumental magnitudes (of the target, the five comparison stars, and their average), and the differential photometry between the target and the average comparison.

[11] Heliocentric Julian Date (HJD) is a usual time correction in variable star work, in order that time measurements do not depend on the particular point at the Earth's orbit when they were obtained. Each HJD time is referred as the time the light from the star would have reached the Sun **[10]**.

Working with the spreadsheet it was possible to obtain lightcurves for each observing session, as those presented in Figs. 3 and 4 just for illustrative purpose. The graphs show the obtained differential photometry lightcurves for a given target star (*C-V*, in blue) and corresponding check star (*C-K*, in red), both simultaneously compared to a suitable comparison star. As seen, overall differences in the latter lightcurves are lesser than 0.05 magnitudes, which validate the correctness of the obtained CV lightcurve.

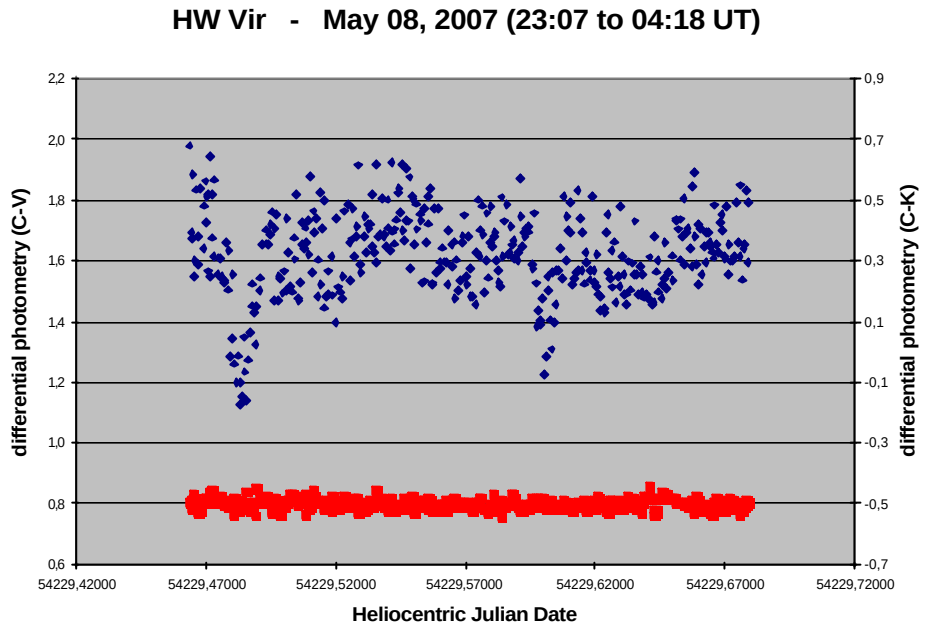

Fig 3
A real large variation of almost 0.9 mag in the HW Vir lightcurve is easily observed.

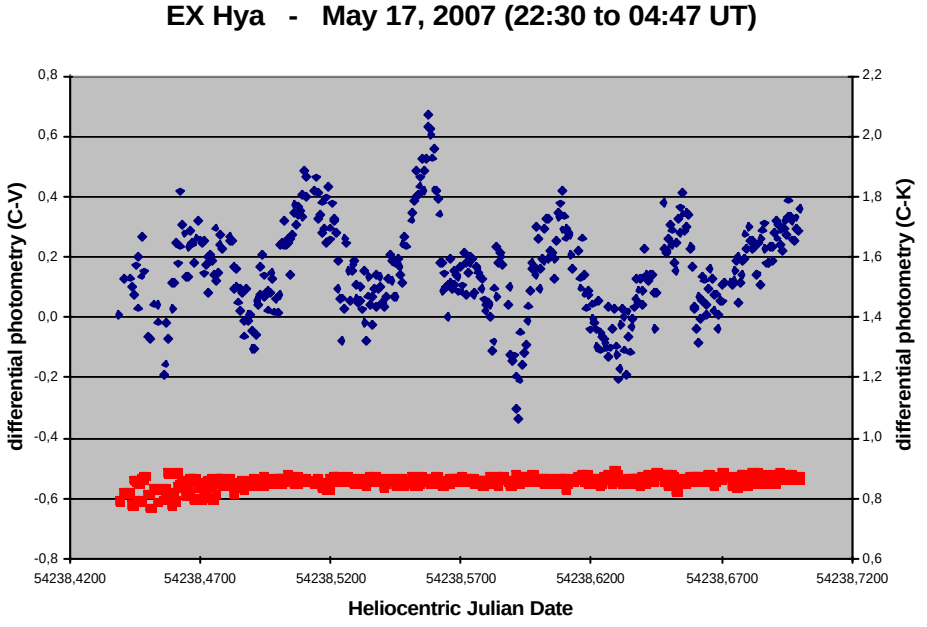

Fig 4
Several cycles are notorious in this interesting lightcurve obtained from EX Hya.

Although both presented lightcurves do show CV variability, there is worthy mentioning difference between them. The HW Vir lightcurve varies roughly between +1.2 and +2.0 mag, while for EX Hya the swing goes from -0.3 to +0.6 mag. This means that HW Vir was measured against an always fainter comparison star (as *C-V* is always positive), which intrinsically enlarges errors (in this case there were no other alternative, as HW Vir was the brightest star in its field).

Performing exactly the same described procedure for all imaging sessions, here are presented without any further treatment (error analysis will be considered in the following section) the obtained lightcurves for HW Vir (after 4 sessions), EX Hya (6 sessions) and V1223 Sgr (2 sessions). Each session has been placed starting just a fixed elapsed time after the ending of the previous one):

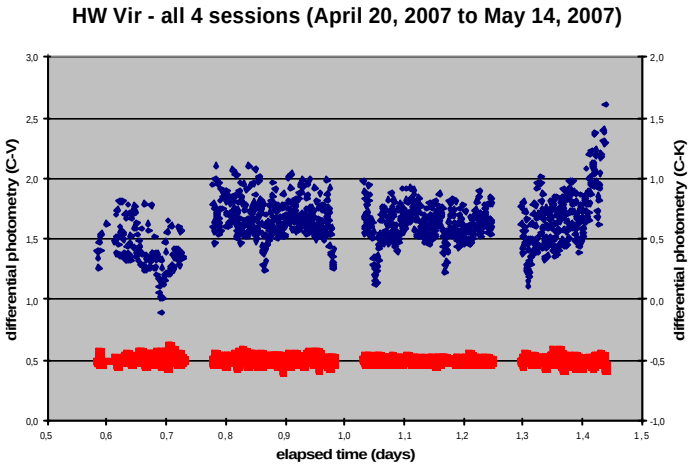

Fig 5
The total obtained lightcurve of HW Vir
(each session is presented separated 0.05 day = 1.2 hs)

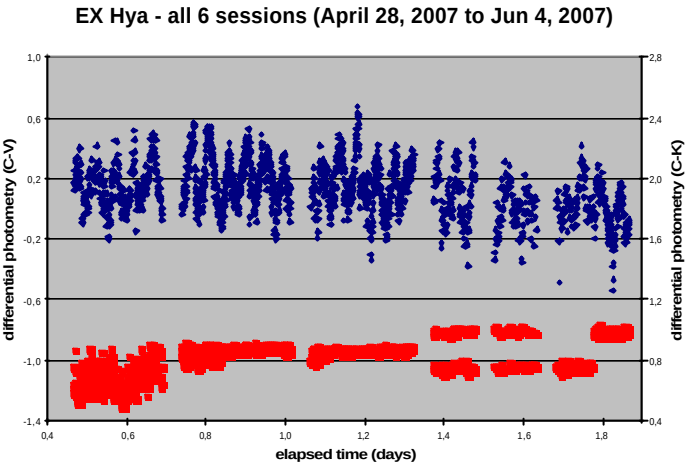

Fig 6
The total obtained lightcurve of EX Hya
(each session is presented separated 0.05 day = 1.2 hs)

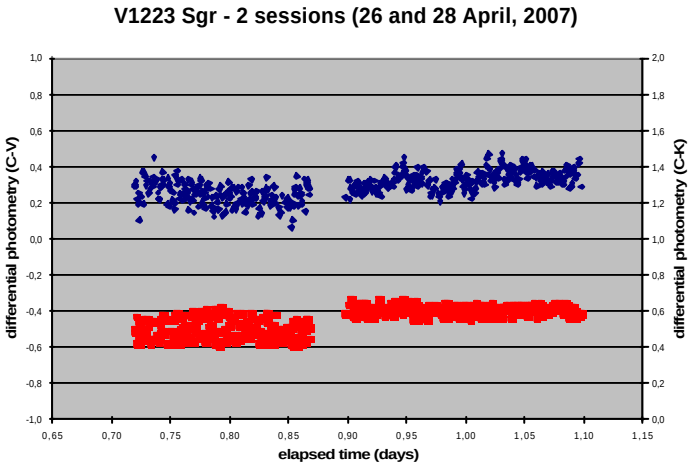

Fig 7
The total obtained lightcurve of V1223 Sgr
(sessions are presented separated 0.03 day = 0.72 hs)

6 – Error estimation for the reduced data

For each EX Hya imaging session the error was estimated as follows. Photometry had been performed by means of five comparison stars. Having selected the one that appeared most stable (for this case, C_3), for each one of the four available C_3-C_i series it was found out its average value and standard deviation, as shown in the following table:

	Session 1		**Session 2**		**Session 3**		**Session 4V**		**S 4R**
	avg	*st dev*	*avg*	*st dev*	*avg*	*st dev*	*avg*	*st dev*	*avg*
C3-C1	1,035	0,122	1,379	0,093	1,415	0,063	1,400	0,021	1,535
C3-C2	0,671	0,092	0,859	0,028	0,857	0,017	0,742	0,020	0,982
C3-C4	1,287	0,144	1,707	0,152	1,761	0,136	2,081	0,025	2,178
C3-C5	0,906	0,122	1,224	0,070	1,238	0,045	1,283	0,020	1,265
	S 4R	**Session 5V**		**Session 5R**		**Session 6V**		**Session 6R**	
	st dev	*avg*	*st dev*	*avg*	*st dev*	*avg*	*st dev*	*avg*	*st dev*
C3-C1	0,018	1,407	0,014	1,525	0,018	1,402	0,025	1,512	0,031
C3-C2	0,015	0,749	0,014	0,989	0,014	0,750	0,018	0,981	0,017
C3-C4	0,056	2,081	0,029	2,164	0,059	1,945	0,104	2,018	0,087
C3-C5	0,017	1,284	0,014	1,245	0,016	1,279	0,025	1,252	0,023

Then, plotting on a graph the absolute value of the average value C_3-C_i versus the standard deviation of C_3-C_i for each imaging session (four pairs of values), it was possible to find out the particular exponential curve (of the type $y = Ae^{Bx}$) that represents the true scattering of such data, as Fig. 8 shows just for two sessions **[11]**. The *A* parameter corresponds to the minimal possible error (when C_3-C_i = 0) and *B* gives and idea of how rapidly the error enlarges when C_3 and C_i were fairly different.

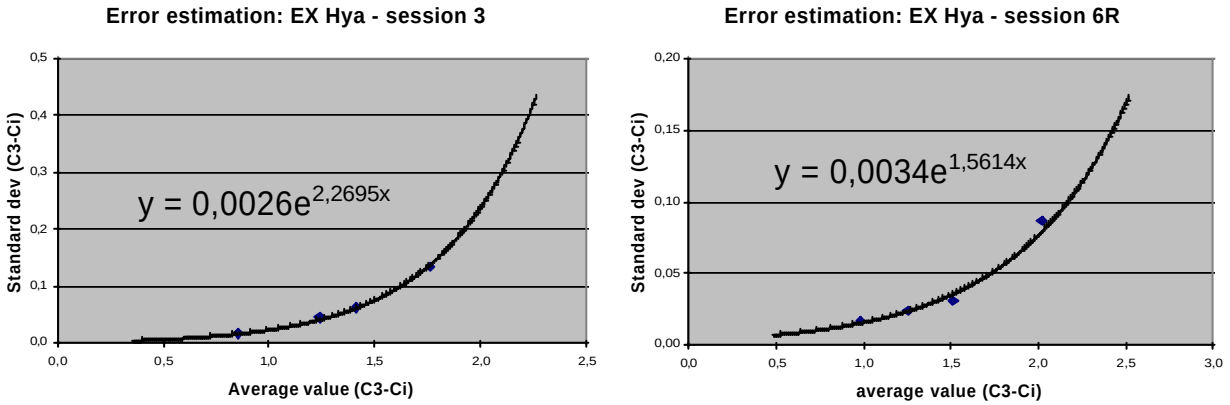

Fig 9
Plotting for each C_3-C_i series the corresponding average value vs the standard deviation in a proper spreadsheet, then it becomes possible to obtain the exponential curve that best fits such values

Once having the *A* and *B* parameters for each imaging session (summarized in the following table), then it became possible to precisely estimate the expected photometry error that prevailed for the particular conditions at that time. The proceeding is simply to apply the corresponding exponential formula to the absolute value of each differential value (in this EX Hya case, C_3-V), in order to find out its corresponding (variable) error.

EX Hya	*Ses 1*	*Ses 2*	*Ses 3*	*S 4V*	*S 4R*	*S 5V*	*S 5R*	*S 6V*	*S 6R*
A	0,0606	0,0056	0,0026	0,0166	0,0044	0,0076	0,0035	0,0046	0,0034
B	0,6895	1,9820	2,2695	0,1830	1,0987	0,5738	1,2489	1,4540	1,5614

For instance, for the session 1 (the one with the highest*A* parameter, something readily expected from observing the great scattering in the check lightcurve that is shown in Fig. 10), the corresponding EX Hya ligthcurve with associated error bars became:

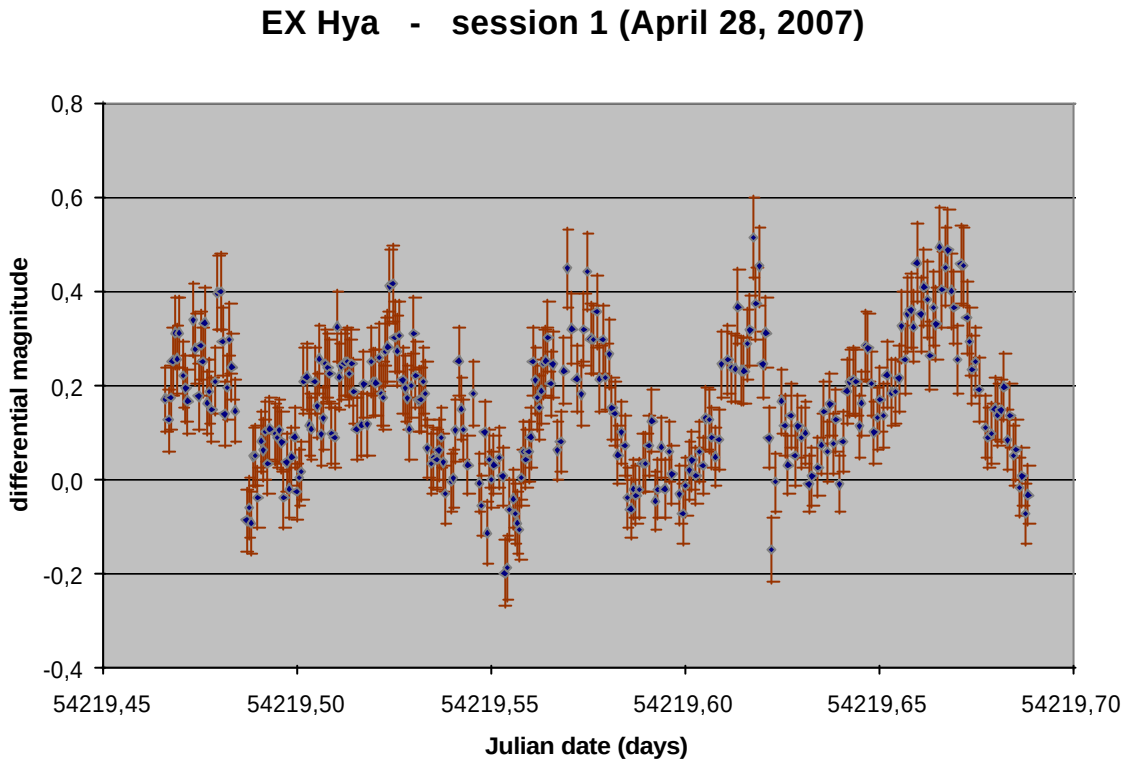

Fig 10
The EX Hya lightcurve obtained from its first imaging session, presenting the associated magnitude error that exactly corresponded to each point of the curve.

A better precision would have been achieved in case more comparison stars were used (a reasonable number being 6 to 10 stars). Anyway, the values obtained for the differential magnitudes among the comparison stars, compared to published data, resulted highly satisfactory. Following is presented such analysis.

Fig. 11a presents a stellar chart centered on EX Hya (just for comparison, Fig 11b is a real image of the same field, one of the literally thousands taken for this work, although one almost without star trailing). The caption of Fig. 11a explains which were the five selected comparison stars, and their respective visual magnitudes. Hence, the real differential magnitudes from all of them could be compared to the same values obtained from this work. Leaving aside those values resulting from photometry performed with the

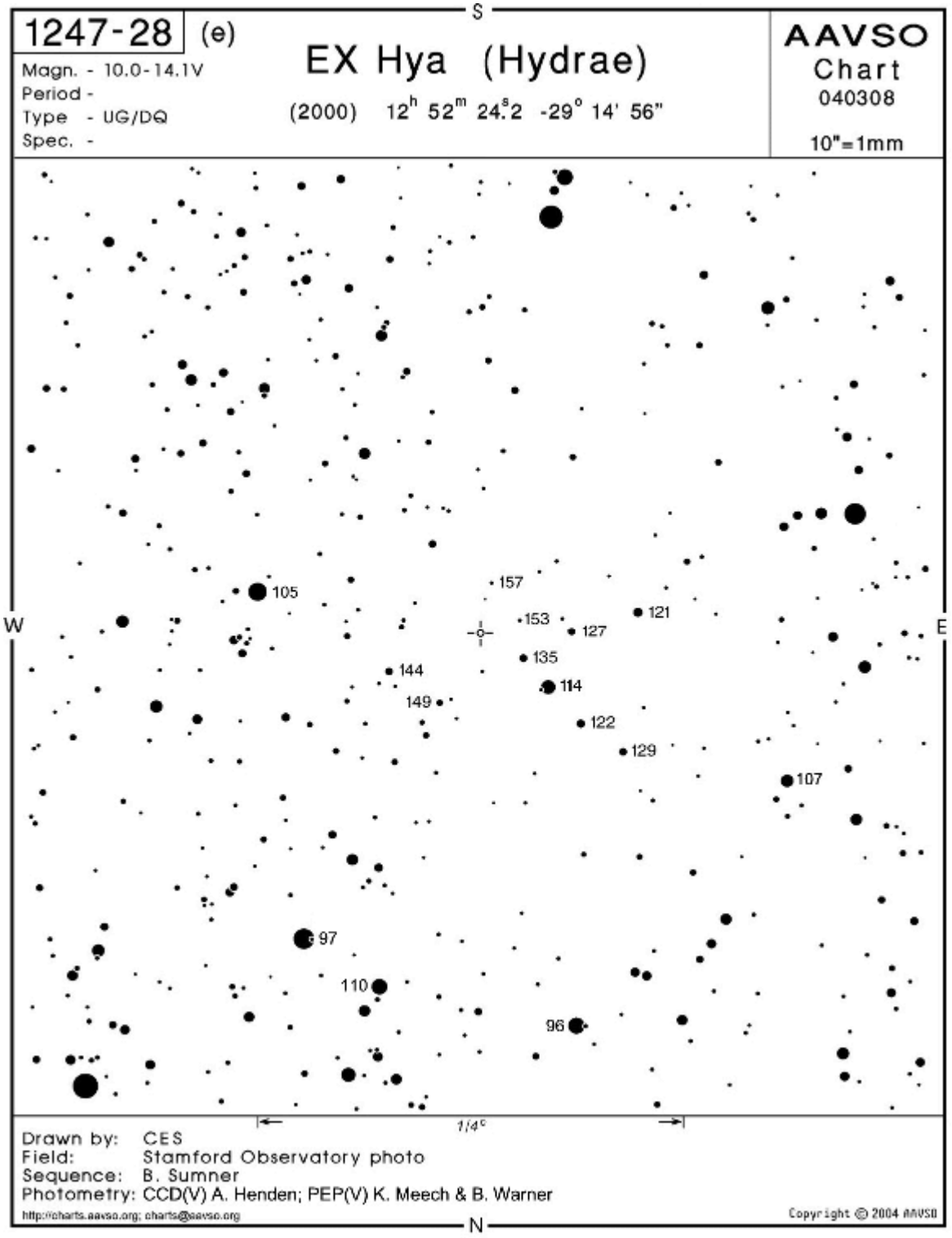

Fig 11a

This stellar chart, centered on EX Hya and matching the same orientation as the images obtained for this work, has been downloaded from AAVSO (the American Association of Variable Star Observers). It presents the visual apparent magnitude of several neighbour stars. In particular, those appearing at the right of EX Hya were selected as the comparison stars (respectively referred as C_1 = 121, C_2 = 127, C_3 = 135, C_4 = 114, and C_5 = 122).

R filter (sessions 4R, 5R, and 6R), all differences were very auspicious with the exception of seccion 1 (not in vain the one with the greatest errors).

EX Hya	***AVVSO***	***Ses 1***	***Ses 2***	***Ses 3***	***S 4V***	***S 4R***	***S 5V***	***S 5R***	***S 6V***	***S 6R***
C3-C1	**1,4**	1,035	1,379	1,415	1,400	1,535	1,407	1,525	1,402	1,512
C3-C2	**0,8**	0,671	0,859	0,857	0,742	0,982	0,749	0,989	0,750	0,981
C3-C4	**2,1**	1,287	1,707	1,761	2,081	2,178	2,081	2,164	1,945	2,018
C3-C5	**1,3**	0,906	1,224	1,238	1,283	1,265	1,284	1,245	1,279	1,252

In particular, the broader differences were for C_3-C_4. The fourth comparison star (C_4) was the brightest one, and due to the poor tracking, the effect of star trailing affected it more negatively than for the fainter ones.

Fig 11b
A real image of the EX Hya, with the same orientation as the stellar chart of Fig. 11a. The FOV is about 22 x 17 arcmin, and the image still lacks of proper flatting correction.

For the remaining monitored CV stars, the error was found in a far more direct way, although not such as accurate. For each image it was calculated the average value of the raw instrumental photometry of the five comparison stars. Then it was found out the

standard deviation of such average corresponding to the whole set of images of one session of a particular target. This last value was taken as the error for such session.

7 – Discussion

The two more important data to extract from the analysis of any single lightcurve is its period and amplitude, in case at least one full cycle has been monitored. While the full amplitude variation is readily obtained, the determination of the period requires a more careful measurement. Also, from the analysis of several lightcurves obtained at different times it may be possible to detect some longer-term variations. Following is such analysis.

a) HW Vir

This *detached* CV star was monitored over four different sessions, spanning four weeks. All lightcurves are presented in Fig. 12 with corresponding error bars. Clearly, data obtained from session 1 and 4 was not so good as those from sessions 2 and 3, although the characteristic peaks due to the bright white dwarf becoming momentarily eclipsed by its fainter companion are still noticed.

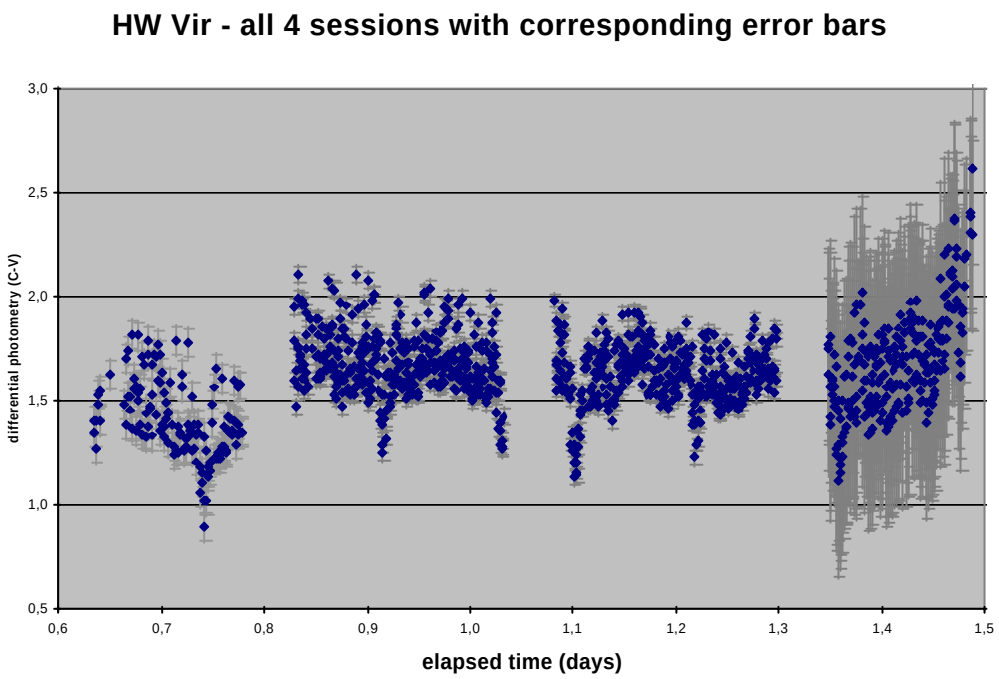

Fig 12
The full lightcurve obtained for HW Vir from 4 monitoring sessions. Error bars correspond to the overall scattered data (standard deviation) of each session. Clearly some problem occurred at session 4.

Data from session 3 was the best one, with standard deviation of just 0.032 magnitudes; on the other hand, correspondent values for session 1 and 4 were respectively 0.067 and 0.461 magnitudes. In particular, humidity during session 4 was exceptional high, at a point that dew began to accumulate at the telescope and finally refrained further imaging, something that never before (or after that) had occurred at OLASU.

The orbital period was obtained by measuring the elapsed time between two consecutive eclipsing peaks. The following table presents the corresponding times for such peaks:

HW vir	***JD of the 1st peak***	***JD of the 2nd peak***	***Elapsed time (days)***
Session 1	2454210,58603	2454210,69203	0,10600
Session 2	2454217,57847	2454217,69494	0,11647
Session 3	2454229,48551	2454229,60018	0,11467
Session 4	2454235,43559	2454235,55428	0,11818

Averaging elapsed times, a first rough value of 0.114 days was obtained. In order to refine it, the second step was to find out how many cycles would have occurred from the last peak of one session to the first peak of the next one, if the orbital period were exactly 0.114 days. It gave:

HW vir	***Time diff (days)***	***Cycles (0,114 d)***	***Cycles (0,1167 d)***
Last peak S 1 to first peak S 2	6,88644	60,41	59,01
Last peak S 2 to first peak S 3	11,79057	103,43	101,03
Last peak S 3 to first peak S 4	5,83541	51,19	50,00

The last step was to find out which exact period, close to 0.114 days, made that each number of cycles between following-up sessions were a round number. By trial and error this exact period was finally found out to be $P = 0.1167$ days = 2.801 hours. The published data for the period of HW Vir is 0.1167195 days with an error of 4×10^{-7} **[12]**. Therefore, the obtained period was remarkable good (a difference of only 2 seconds). Fig. 13 presents the "true" lightcurve obtained by professional astronomers **[12]**.

Due to orbital eclipses, the observed variation in amplitude of HW Vir was about 0.4 magnitudes for all the 4 sessions. Considering the poor quality of data from session 1 and 4 (the two furthest separated in time), nothing can be said about any observed "week-term" variability (although detached CVs as HW Vir should be fairly stable).

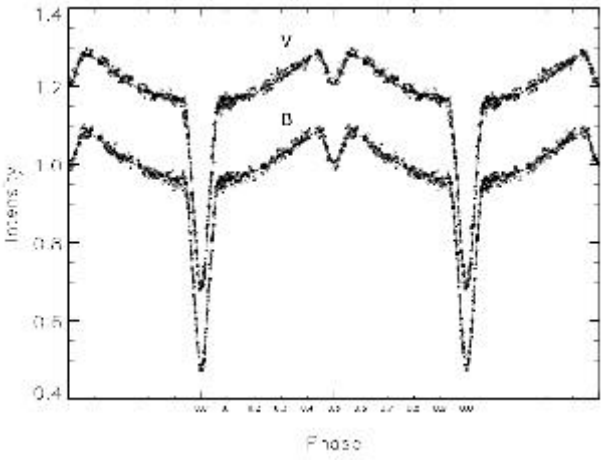

Fig. 13
The "professional" B and V lightcurves of HW Vir. The V lightcurve appears shifted 0.25 on the ordinate, just to facilitate the visualization of both curves.

b) EX Hya

Conversely to the "easy" detached system of HW Vir, the case of the *intermediate polar* EX Hya is far more interesting – and complicated. In intermediate polars the medium-strength field of the CV star does interact with the accretion flow, making the white dwarf to become spun up by the accretion of material and thus losing its synchronism with respect to the orbital period – becoming no longer *tidally locked* **[13]**.

Fig. 14 shows the monitoring outcome obtained after a total span of six weeks. This CV star shows large amplitude variations (about 0.6 mag) in short time (the dream of the any variable star investigator). The corresponding bar errors have been calculated for each single point, as explained in the previous section. All data look essentially valid.

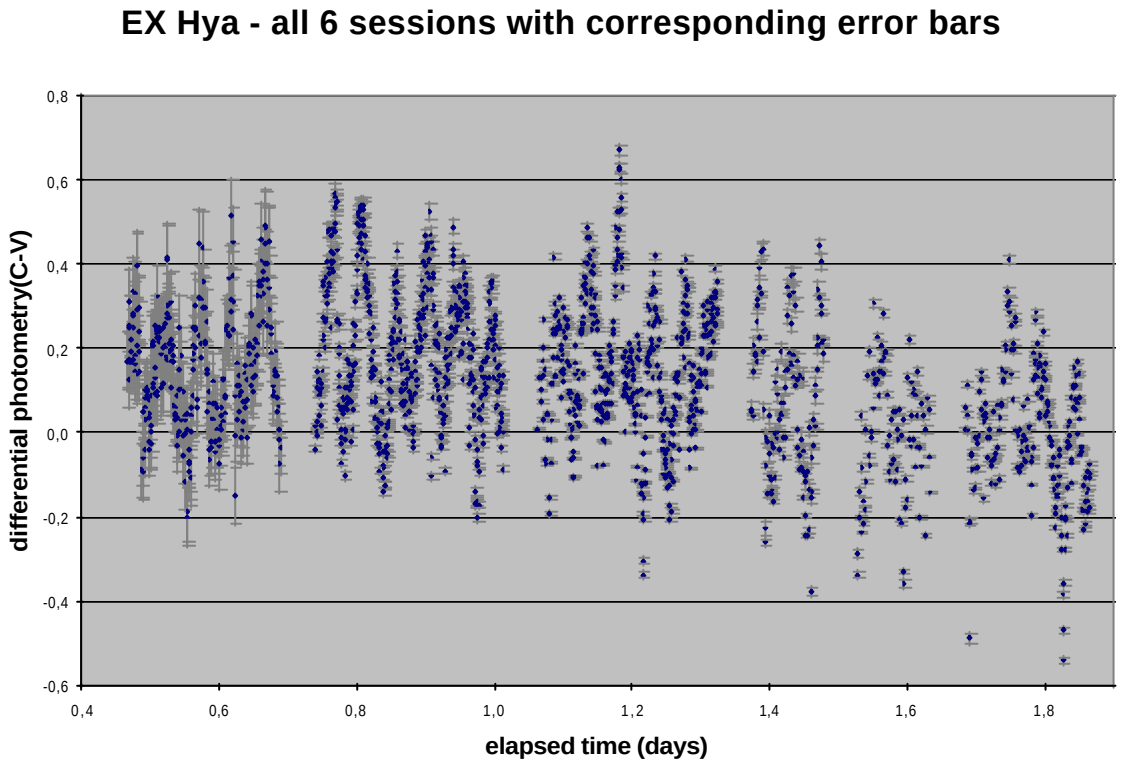

Fig 14
The lightcurves obtained from EX Hya during a total monitoring span of six weeks. The initial three sessions corresponded to unfiltered images (thus requiring lesser exposures times), while photometric filters V and R were used for the last three sessions.

The first notorious issue about EX Hya's lightcurves is the presence of a lot of short and well-defined maximums (points of increased luminosity), totally absent for the case of HW Vir. This is due to the accretion disk (the detached HW Vir has no accretion disk at all) which can be very bright, in particular at the *bright spot* – the place where the flow from the secondary hits the disk edge. In fact, such bright spot is usually brighter that the white dwarf itself.

Therefore, the two fundamental periods of this CV star, the one due to the spin of the white dwarf and its bright accretion disk – EX Hya's *"day"* – plus the other due to the truly orbital revolution –EX Hya's *"year"* –both appeared tangled in the lightcurves. Luckily, the two different periods were still possible to be untangled, as the former corresponds to the appearance of the bright spot (relative maximums), while the latter to the occurrence of orbital eclipses (relative minimums, the same as for HW Vir).

Finding out the time difference (in days) for two consecutive relative maximums for sessions 1, 2 and 3, it resulted:

EX Hya	***1st cycle***	***2nd cycle***	***3rd cycle***	***4th cycle***	***5th cycle***	***average***
Session 1	0,04432	0,04740	0,04562	0,04791	-	**0,04631**
Session 2	0,03996	0,05111	0,04452	0,05177	0,04072	**0,04562**
Session 3	0,04727	0,04712	0,05150	0,04609	0,04508	**0,04741**

Thus, by obtaining the grand average for the 14 cycles the resulting spin period was 0.04646 days = 66.9 minutes. The actual spin period recently measured is 4021.6 seconds **[14]**, that is, 67.027 minutes, so that the obtained value has 0.2 % accuracy.

The orbital period was not so easy to find. Fig. 15 simultaneously presents the four longest sessions obtained for EX Hya, plotted conveniently displaced in the vertical scale (session 6V and 6R were also conveniently matched). By selecting session 2 (the longest) as the reference, sessions 1, 3 and 4 were also displaced horizontally until obtaining a fair matching for some relative minimums (those at about 0.04, 0.11, 0.18, and 0.25 days. This was the key that opened the door to the orbital period.

Finding out the time difference (in days) for two consecutive relative minimums for sessions 1, 2, 3 and 6, it resulted:

EX Hya	***1st cycle***	***2nd cycle***	***3rd cycle***	***average***
Session 1	0,06599	0,06821	0,06532	**0,06651**
Session 2	0,06199	0,07073	0,06729	**0,06667**
Session 3	0,06800	0,06782	0,06878	**0,06820**
Session 6	0,07268	0,06328	-	**0,06798**

Thus, by obtaining the grand average for the 11 cycles the resulting orbital period was 0.06728 days = 96.9 minutes. The actual orbital period recently measured is 5895.4 seconds **[14]**, that is, 98.257 minutes, so that the obtained value has 1.4 % accuracy.

Examining Fig. 14 for detecting any long-term variability over the full monitored lapse (six weeks), in the last three sessions it appeared a tendency to decrease the average brightness of EX Hya.

Finally, an interesting analysis could be made from the fact that the last three sessions were performed with photometric filters V and R. Fig 16 presents side by side the outcome of sessions 4 and 5, where both filters were used alternatively (that is, permitting to obtain the V-lightcurve and the R-lightcurve for the same EX Hya's variability. The scales for both graphs are exactly the same.

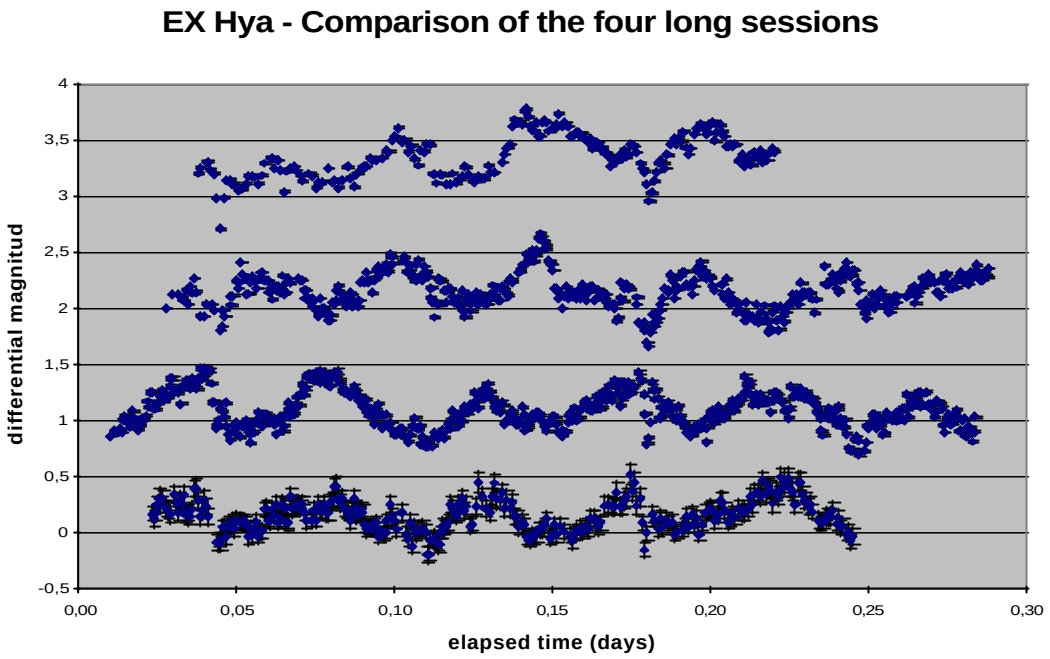

Fig 15

EX Hya' sessions 1, 2, 3 and 6 (the longest ones) appear displaced vertically from the lowest position, with session 6R also matched to session 6V by been shifted an additional 0.3 mag. They were compared in order to detect the elusive orbital period by looking for the repetitive coincidence of relative minimums (orbital eclipses). Finally, the coincidence appeared as shown in the graph for elapsed times around 0.04, 0.11, 0.18 and 0.25 d.

The first conclusion is that the V-curve (in green) is brighter than the R-curve (in red), despite that the sensitivity of the imaging system – filter included – is 4 % larger for red wavelengths (0.738 at 600 nm) than for visual wavelengths (0.712 at 520)[12].

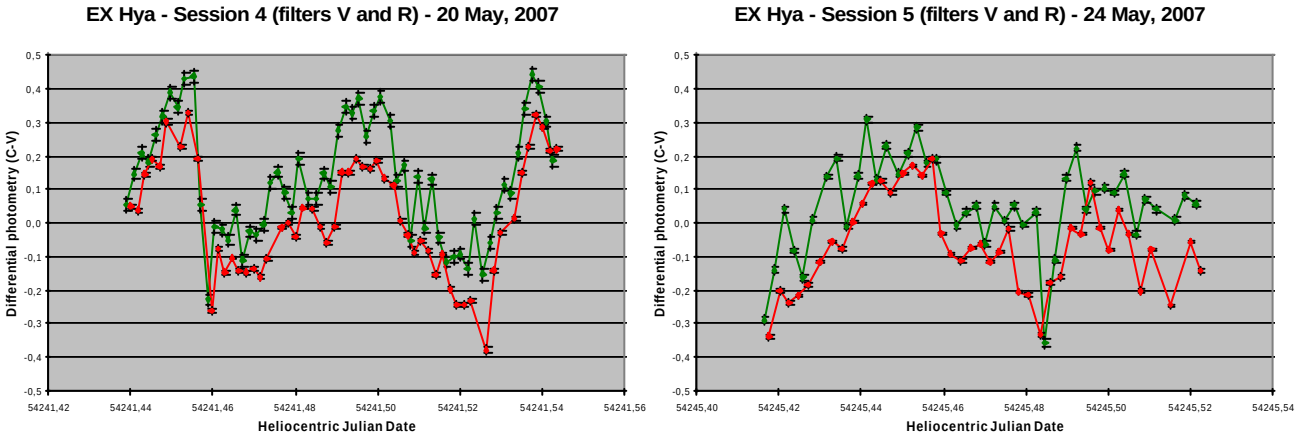

Fig 16

The V- and R-ligthcurves of EX Hya (respectively in green and red) obtained in two different sessions, with corresponding error bars. The curve of the left nicely shows one full orbital cycle and two full spinning cycles, while for the right curve it only appears one cycle of each type.

[12] Both factors have been obtained by multiplying the corresponding transmission numbers for the telescope, the CCD camera, and the filters, whose transmission curves and computation are given in Appendix I.

The V-R magnitude of the comparison star (obtained by averaging the data from the three filtered sessions) is + 0.217 mag, that is, it is brighter in red than in visual wavelengths. The average of the V-R lightcurves is roughly about + 0.1 mag. Therefore, the whole EX Hya system has to be brighter at visual wavelengths that at red.

In three of the four observed orbital eclipses, the V- and R-values are almost the same, that is, at eclipses there is a larger brightness decreasing for V than for R. This means that the bright covered star (the white dwarf) is brighter at visual than at red wavelengths (as it should be).

EX Hya's lightcurve obtained by professional astronomers **[15]** is shown in Fig. 17.

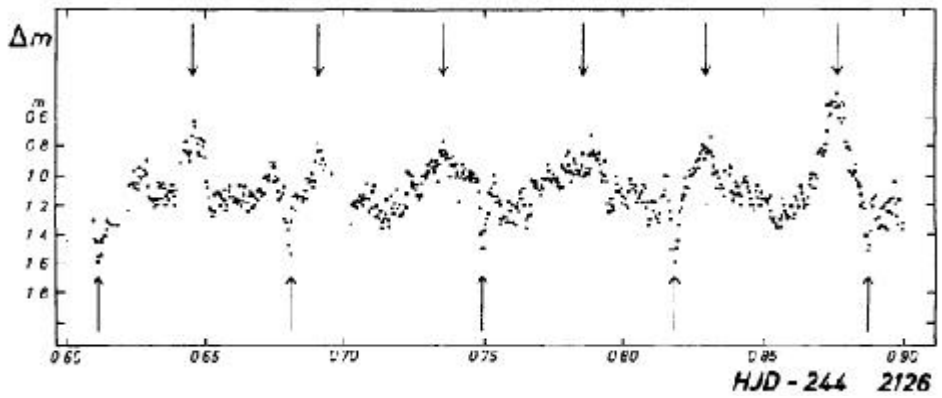

Fig 17
The "professional" lightcurve of EX Hya. Going-down arrows indicate those relative peaks that correspond to the spin period, going-up arrows those of the orbital period.

c) V1223 Sgr

Another intermediate polar, although much fainter than EX Hya and also with lesser changes in amplitude. As Fig. 7 shows, the quality of data is not very good, as the variation of the C-V photometry is barely bigger than the dispersion of the C-K values. Surely it has a very short spin period, which difficult the task of measuring both periods.

d) T Pyx

This originally selected target was shortly abandoned because at the "large" CCD field used for this project it appeared very close to another star of almost the same magnitude. When photometry was intended, it became impossible to separate one star from the other (the software autocorrects the position, always embracing both stars).

e) AB Nor

This CV star resulted too faint for good photometry processing. Despite having taken 329 images during almost four hours, all the work was useless.

Conclusions

Two cataclysmic variables stars (HW Vir and EX Hya) were especially monitored during about a month in order to obtain scientific data from standard amateur equipment. After careful image processing, differential photometry based on the comparison to several nearby stars allowed obtaining their respective lightcurves, with especial emphasis in the measuring of photometry errors.

From analysis of those lightcurves it was possible to obtain the orbital period of such interacting binary stars, with an excellent precision. Also, the spin period of EX Hya and some deductions about the physical properties of the systems could be found out.

Despite the hard work and large time consumed by this project, the bottom line is that it has been a highly rewarding experience. The author has proved himself that there is a truly scientific potential within his reach, only on condition that the labour has to be properly and unhurriedly performed.

References

[1] Alan MacRobert, *"A Dwarf Nova's Spectacular Past"*, Sky & Telescope, July 2007, page 16
[2] Coel Hellier, "*Cataclysmic Variable Stars – How and why they vary"*, Springer – Praxis Publishing, 2001, page 1
[3] Bradley W. Carroll and Dale A. Ostlie, *"An Introduction to Modern Astrophysics"*, 2nd ed, Pearson Publishing, 2007, page 672
[4] H. Ritter and U. Kolb, *"The Catalogue of Cataclysmic Binaries"*, ed 7.7, 2006, at Ritter H., Kolb U. 2003, A&A, 404, 301 (update RKcat7.7)
[5] Ron Wodaski, *"The New CCD Astronomy"*, New Astronomy Press, 2002, page208
[6] Brian D. Warner, *"A Practical Guide to Lightcurve Photometry and Analysis"*, Bdw Publishing, 2003, page 32
[7] Gerald North BSc., *"Advanced Amateur Astronomy"*, Cambridge University Press, 2nd ed, 1997, page 90
[8] Brian D. Warner, *"A Practical Guide to Lightcurve Photometry and Analysis"*, Bdw Publishing, 2003, page 30
[9] Richard Berry and James Burnell, *"The Handbook of Astronomical Image Processing"*, 2nd ed, Willmann-Bell, Inc, 2005, pages 279-290
[10] Brian D. Warner, *"A Practical Guide to Lightcurve Photometry and Analysis"*, Bdw Publishing, 2003, page 65
[11] Paddy McGee, private communications during May, 2007, plus "*Error estimation in differential photometry"* at http://www.physics.adelaide.edu.au/~pmcgee/error.htm
[12] C. Ibanoglu, O. Cakirh, G. Tas, and S. Evren, "*High-speed photometry of the pre-cataclysmic binary HW Virginis and its orbital period change"*, Astronomy & Astrophysics, Vol 414, 2004, pages 1043-1048
[13] Coel Hellier, "*Cataclysmic Variable Stars – How and why they vary"*, Springer – Praxis Publishing, 2001, page 127
[14] K. Beuermann, Th.E. Harrison, B.E. McArthur, G.F. Benedict, and B.T. Gansicke, *"A precise HST parallax of the cataclysmic variable EX Hya, its system parameters, and accretion rate"*, Astronomy & Astrophysics, Vol 412, 2003, pages 821-827
[15] N. Vogt, W. Krzeminiski, and C. Sterken, *"Periodic and Secular Variations in the Lightcurve od Dwarf Nova EX Hydrae"*, Astronomy & Astrophysics, Vol 85, 1980, pages 106-112

Appendix I

The transmission curves for the used imaging system

The curve for the telescope Meade LX200R with UHTC (upper curve):

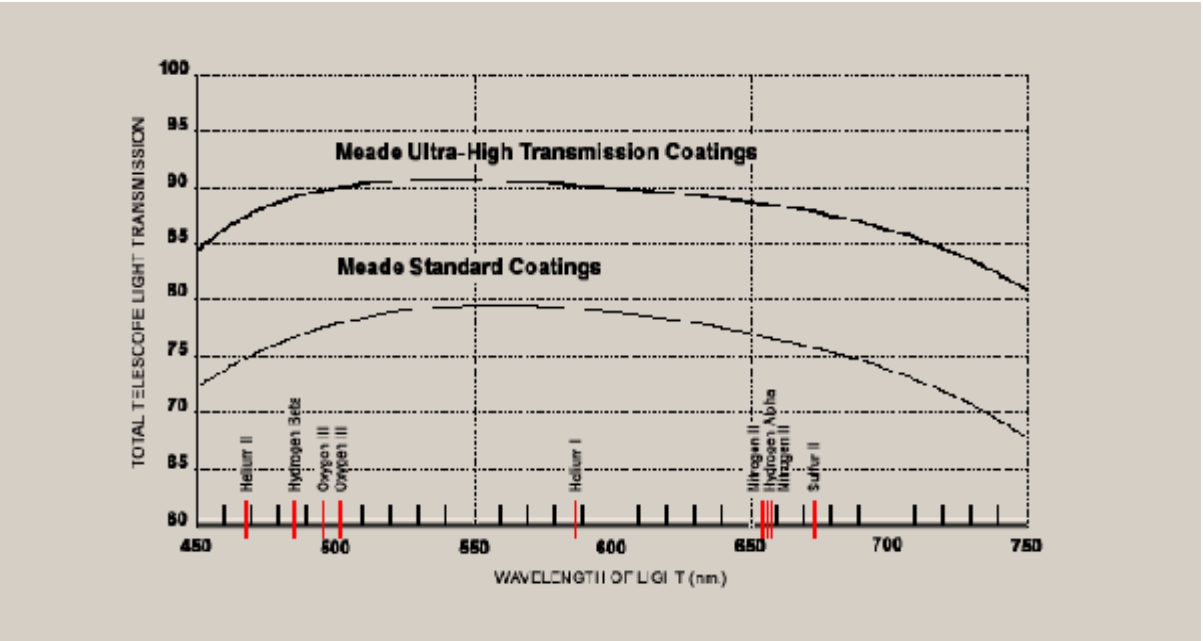

*Credit: Meade Instrument Corporation (*http://www.meade.com/catalog/uhtc/index.html*)*

The curve for the CCD camera Meade DSI PRO II:

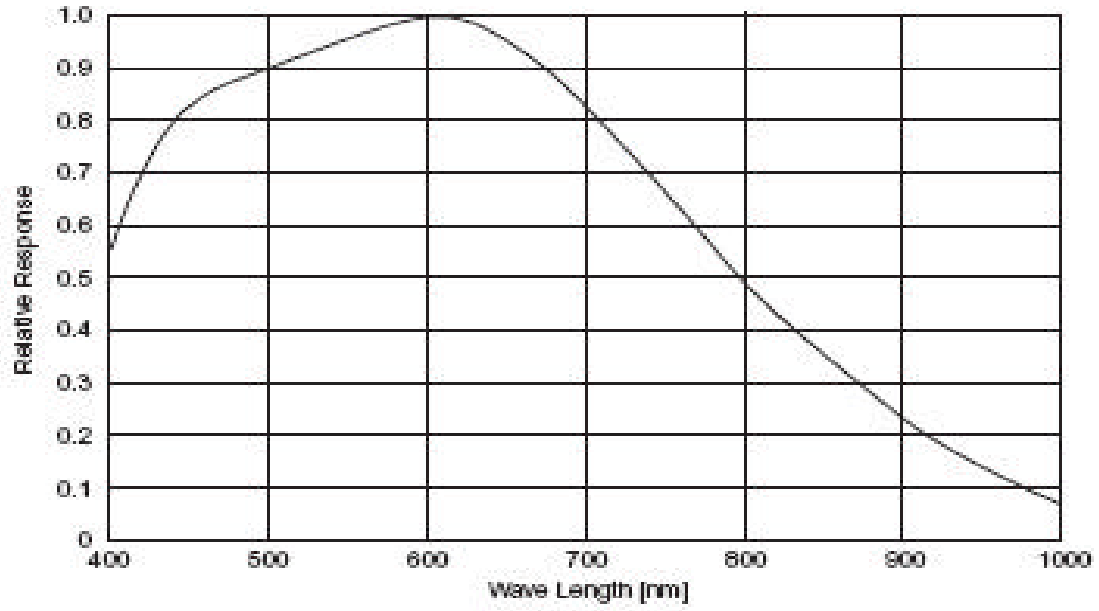

Credit: Sony Corporation (http://products.sel.sony.com/semi/PDF/ICX429ALL.pdf)

The curves for the photometric filters Astrodon :

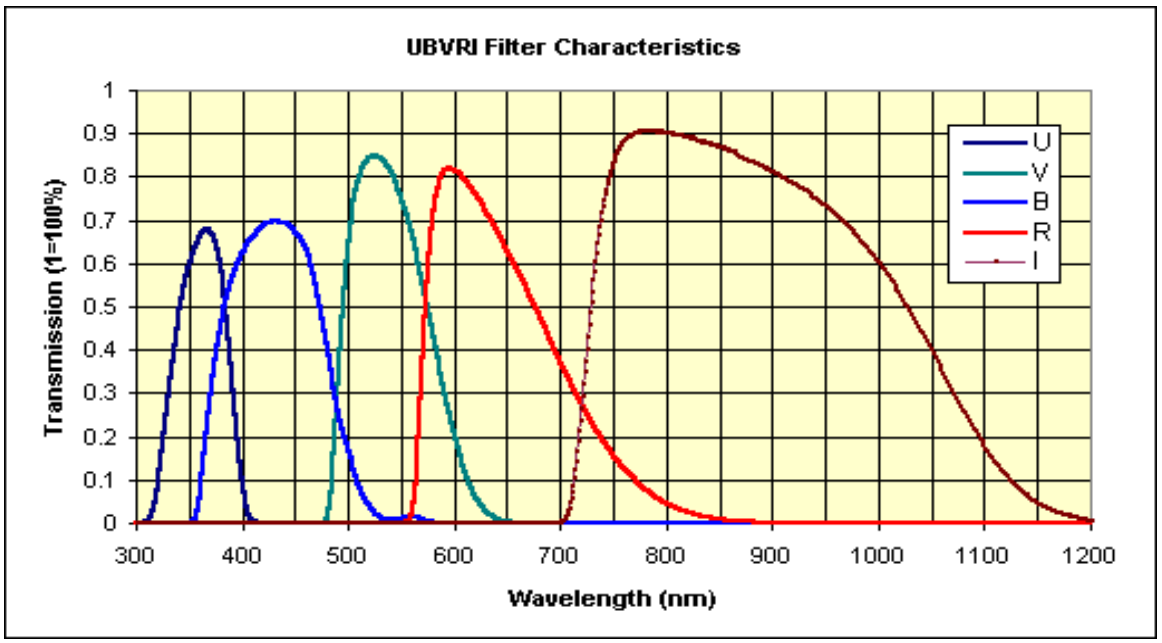

*Credit: Astrodon (*http://www.sbig.com/products/filters.htm#UBVRI*)*

Therefore, the combined attenuation (*) gives:

	telescope	***CCD camera***	***filter***	***overall factor***
Visual (520 nm)	0,91	0,92	0,85	0,712
Red (600 nm)	0,90	1,00	0,82	0,738

(*) The incidence of the focal reducer has not been included, since no available curve could be found.

Appendix II – The log of all imaging activities performed for this project (autumn 2007)

target	*Apr 19*	*Apr 26*	*Apr 28*	*May 08*	*May 09*	*May 14*	*May 17*	*May 20*	*May 24*	*Jun 04*
T Pyx	20:29-22:12 1.7 hs 55 imag unfiltered 60 sec									
HW Vir	*Session 1* 23:01-02:28 3.6 hs 160 imag unfiltered 60 sec	*Session 2* 20:47-01:41 4.8 hs 424 imag unfiltered 30 sec		*Session 3* 20:07-01:18 5.2 hs 432 imag unfiltered 42.4 sec		*Session 4* 19:11-23:13 4.0 hs 290 imag unfiltered 42.4 sec				
AB Nor	02:44-06:22 3.6 hs 329 imag unfiltered 30 sec									
V1223 Sgr		*Session 1* 02:14-05:48 3.5 hs 250 imag unfiltered 42.4 sec	*Session 2* 01:47-06:36 4.8 hs 314 imag unfiltered 42.4 sec							
EX Hya			*Session 1* 20:10-01:30 5.3 hs 292 imag unfiltered 42.4 sec		*Session 2* 19:30-02:05 6.5 hs 541 imag unfiltered 42.4 sec		*Session 3* 19:30-01:47 6.2 hs 490 imag unfiltered 42.4 sec	*Session 4V* 19:31-22:00 2.5 hs 60 imag filter V 60 sec *Session 4R* 19:32-22:02 2.5 hs 60 imag filter R 60 sec	*Session 5V* 18:54-21:14 2.4 hs 41 imag filter V 84.9 sec *Session 5R* 18:56-21:16 2.4 hs 41 imag filter R 84.9 sec	*Session 6V* 20:03-22:23 2.3 hs 94 imag filter V 84.9 sec *Session 6R* 22:25-24:29 2.1 hs 120 imag filter R 60 sec